学 位 論 文

In vivo hypoxia imaging of brain tumors can visualize microscopic necrosis and anaerobic glycolysis.

（脳腫瘍に対するインビボ低酸素イメージングによって腫瘍内の顕微鏡的壊死や嫌気性糖代謝を可視化する）

2017 年 3 月

北 海 道 大 学

豊永　拓哉

学 位 論 文

In vivo hypoxia imaging of brain tumors can visualize microscopic necrosis and anaerobic glycolysis.

（脳腫瘍に対するインビボ低酸素イメージングによって腫瘍内の顕微鏡的壊死や嫌気性糖代謝を可視化する）

2017 年 3 月

北 海 道 大 学

豊永　拓哉

目次

List of publications and presentations

Publications

Toyonaga T, Hirata K, Yamaguchi S, Hatanaka C. K, Yuzawa S, Manabe O, Kobayashi K, Watanabe S, Shiga T, Terasaka S, Kobayashi H, Kuge Y, Tamaki N.
^{18}F-fluoromisonidazole positron emission tomography can predict pathological necrosis of brain tumors.
European Journal of Nuclear Medicine and Molecular Imaging
July, 2016;43(8):1469-76.

Toyonaga T, Yamaguchi S, Hirata K, Kobayashi K, Manabe O, Watanabe S, Terasaka S, Kobayashi H, Hattori N, Shiga T, Kuge Y, Tanaka S, Ito M. Y, Tamaki N.
Hypoxic glucose metabolism in glioblastoma as a potential prognostic factor.
European Journal of Nuclear Medicine and Molecular Imaging
In press.

Presentations

Toyonaga T, Hirata K, Kobayashi K, Manabe O, Hattori N, Shiga T, Yamaguchi S, Kuge Y, Huang N, Tamaki N.
Hypermetabolic fraction of hypoxic volume may help predict prognosis in patients with glioblastoma multiforme.
Society of Nuclear Medicine and Molecular Imaging 2015 Annual meeting
July, 2015. Baltimore, Maryland, USA.

Toyonaga T, Yamaguchi S, Kobayashi K, Manabe O, Hirata K, Hattori N, Shiga T, Hatanaka C. K, Yuzawa S, Tamaki N
18F-FMISO PET can predict the pathological necrosis of brain tumor.
Society of Nuclear Medicine and Molecular Imaging 2015 Annual meeting
June, 2015. Baltimore, Maryland, USA.

Toyonaga T, Kobayashi K, Manabe O, Hirata K, Hattori N, Shiga T, Terasaka S, Kobayashi H, Tanaka S, Tamaki N.
Hypoxic imaging for assessing brain tumor using 18F-FMISO PET.
The 15th Asian Oceanian Congress of Radiology 2014
September, 2014. Kobe, Japan.

Introduction

Hypoxia is well known as one of the major factors that affect tumor malignancy. Hypoxic conditions stabilize the hypoxia inducible factor (HIF) in malignant tumor cells. HIF-1α forms a complex with HIF-1 or with other proteins, and adheres to hypoxia responsive elements (HRE; i.e., 5′-ACGTG-3′) on the genome line. HRE stimulates many of downstream proteins concerning about the glycolytic system, cell migration, angiogenic signaling, and cell proliferation[1]. In addition, hypoxia is well known to induce radiation resistance, because free radical-induced DNA damage requires oxygen molecules[2]. Lactate is produced by anaerobic glycolysis and may scavenge superoxide and hydroxyl radicals[3]. Hypoxia also induces resistance to many types of chemotherapy. Temozolomide, which is the main treatment agent against high-grade glioma, reduces its treatment effect under hypoxia[4]. It is reasonable that tumor hypoxia causes poor prognosis by means of such treatment resistance.

Fluoromisonidazole (FMISO) is the most widely used tracer of positron emission tomography (PET) to visualize severe hypoxia *in vivo*. It is a derivative of misonidazole (MISO) that is used as a radiosensitizer[5]. Unfortunately, mainly because of cytotoxicity, MISO has not been used in clinical settings for treatment purposes[6]. Subsequently, FMISO was developed as a hypoxia imaging PET tracer[7,8]. Several studies have suggested that FMISO accumulation sharply increases under the condition of partial pressure of oxygen (pO2) less than 10–20 mmHg[8,9].

To elucidate whether FMISO PET can visualize tumor malignancy in vivo, we evaluated the correlation between FMISO uptake and histopathological malignant finding or clinical prognosis. We previously showed that FMISO accumulation related with presence of necrosis and allow distinguishing glioblastoma from other lower-grade gliomas[10]. Thus, in chapter 1, we focus on the relationship between hypoxia and necrosis not only for astrocytic glioma but also for other types of brain tumor, including lymphoma and metastatic brain tumors. We tested the diagnostic performance of FMISO to predict pathological diagnosis in terms of present/absent necrosis.

In chapter 2, we focus on the FMISO-and-fluorodeoxyglucose (FDG) double positive area, where we assume anaerobic glycolysis may be dominant for energy production. Previous studies reported the correlation between the hypoxia volume (HV) and prognosis of glioma patients[11,12]. However, there may be biologically heterogeneity inside the FMISO-positive area, containing necrotic or dying cells, and active tumor cells that adapt to severe conditions. Theoretically, tumor aggressiveness should be ascribed only to the viable cell fraction. Thus, we tested whether the parameters from FMISO-and-FDG double positive area have a potential to predict prognosis.

List of Abbreviations

3D-SPGR	three-dimensional spoiled gradient echo
AA	anaplastic astrocytoma
AE	anaplastic ependymoma
AO	anaplastic oligodendroglioma
AOA	anaplastic oligoastrocytoma
CT	computed tomography
DA	diffuse astrocytoma
EOR	extent of resection
FDG	^{18}F-fluorodeoxyglucose
FLAIR	fluid-attenuated inversion recovery
FMISO	^{18}F-fluoromisonidazole
Gd	gadolinium
Gd-T1WI	gadolinium-enhanced T1-weighted imaging
GTV	gross tumor volume
HIF	hypoxia inducible factor
HMF	hypermetabolic fraction of hypoxia volume
hMTV	hypoxic metabolic tumor volume
HRE	hypoxia responsive elements
hTLG	hypoxic total lesion glycolysis
HV	hypoxia volume
LYG	lymphomatoid granulomatosis
MISO	misonidazole
MRI	magnetic resonance imaging
MTV	metabolic tumor volume
OA	oligoastrocytoma
OL	oligodendroglioma
OS	overall survival
PCNSL	primary central nervous system lymphoma
PET	positron emission tomography
PFS	progression-free survival
ROC	receiver operating characteristic
ROI	regions of interest
SD	standard deviation
SUV	standardized uptake value
TNR	tumor-to-normal cerebellum ratio
VOI	volume of interest
WHO	World Health Organization

Chapter 1

Purpose

Several subtypes of brain tumor develop intratumoral necrosis, and the presence of necrosis is usually an indicator of malignancy or a prognostic factor[13-16]. Tumor necrosis is well correlated to the mitotic index, increases in cellularity, and a high nucleus to cytoplasm ratio. These findings suggest that necrosis might be correlated to tumor progression and therefore prognosis. Ring-like enhancement of contrast-enhanced computed tomography (CT) and magnetic resonance imaging (MRI) can detect macro-necrosis, but only histopathological examination can detect micro-necrosis. Tumor sampling is no doubt an important method to accurately evaluate tumor characteristics. In contrast, the invasiveness of tumor sampling is a clinical obstacle. Non-invasive prediction of the presence of necrosis would highly affect the treatment strategy.

Hypoxia is well known as a major factor in the induction of necrosis. We hypothesized that FMISO PET could identify intratumoral necrosis not only in gliomas but also any type of brain tumor. To test this hypothesis, we applied FMISO PET to subjects with various types of brain tumors before tumor resection, and evaluated the correlation between histopathological necrosis and FMISO accumulation. We also evaluated the threshold of semi-quantitative values in these subjects, which might predict the presence of necrosis.

Materials and methods

Patients

We reviewed a total of 176 FMISO PET scans from 141 patients for the investigation of possible brain tumors at Hokkaido University Hospital. The chapter 1 study included brain tumor patients who underwent FMISO PET before radiation therapy, chemotherapy, and surgical intervention. Patients who had not undergone tumor resection or biopsy after PET examinations were excluded. We father excluded the cases of which we could not collect the surgical specimens. Overall, the study population included 66 patients (M:F=36:30, age: 27–85 years). Surgeries were performed at Hokkaido University Hospital or our affiliated hospitals. Detailed surgical procedures are described below. Surgical specimens were collected by the Department of Pathology at Hokkaido University. The study was approved by the Ethics Committee of Hokkaido University Hospital. Written informed consent was obtained from all patients.

Imaging protocol

All patients underwent MRI and FMISO PET before surgical intervention. MRI sequences included T1-weighted with and without gadolinium enhancement, T2-weighted, and fluid-attenuated inversion recovery (FLAIR) images. The types of MRI scanners depended on the facility.

For FMISO PET, patients were not asked to fast before the study. Static PET scanning was initiated at 4 hours after intravenous injection of 400 MBq FMISO (406.42 ± 35.45 MBq) as recommended previously[17,18]. PET scanners used in this study were an ECAT HR+ PET scanner (Asahi-Siemens Medical Technologies Ltd., Tokyo, Japan), Biograph 64 PET-CT scanner (Asahi-Siemens Medical Technologies Ltd., Tokyo, Japan), and Gemini TF64 TOF-PET/CT scanner (Hitachi Medical Corporation Ltd, Tokyo, Japan). All scanners were operated in the three-dimensional mode. For the ECAT HR+ scanner, the 10-minute emission acquisition was followed by 3 minute transmission scanning with a 68Ge/68Ga retractable line source. For Biograph 64 PET/CT and Gemini TF PET/CT scanners, the 10 minute emission acquisition was followed by CT scanning for attenuation correction. Attenuation-corrected radioactivity images were reconstructed using filtered back projection (ECAT and Biograph) or the ordered subset expectation maximization method (Gemini) with a Hann filter of 4 mm full-width at half-maximum.

Semi-quantitative analysis

The tumor-to-normal cerebellum ratio (TNR) was calculated for semi-quantitative analysis. First, a nuclear medicine physician (Ta.To.) created 15 10-mm-diameter circular regions of interest (ROIs) (five ROIs on each of the axial slices) on both sides of the cerebellar cortex for a total of 30 ROIs per patient. The average values of these regions of the standard uptake value (SUV) were defined as normal references. The SUV was calculated as [tissue radioactivity (Bq/ml)] × [body weight (g)] / [injected radioactivity (Bq)]. Second, we placed one 30-mm round volume of interest (VOI) containing the voxel of the tumor that showed the highest visual accumulation. The tumor regions were determined with reference to gadolinium-enhanced T1-weighted images. Then, the maximum SUV (SUVmax) of the tumor was divided by averaging the cerebellar SUV as the TNR.

Surgical procedures

The surgical procedure was performed in the same manner as described previously[19,20]. We used an intraoperative neuronavigation system (StealthStation®, Treon® or S7®, Medtronic). Gadolinium-enhanced T1-weighted imaging (Gd-T1WI) with three-

dimensional spoiled gradient echo (3D-SPGR) MR images and PET images were transferred to the navigation system. FDG PET was used to identify the most active tumor tissue, and FMISO PET was used to evaluate hypoxic area. The surgical procedure was either biopsy or tumor resection. When the patients underwent biopsy, the biopsy target was set in the FMISO-uptake lesion using the navigation system in cases of an identified FMISO uptake lesion. When the patients underwent maximum tumor resection, FMISO-accumulated areas were contained in the extent of resection as much as possible.

Pathological classification

According to the pathological diagnosis, brain tumors were divided into three groups: astrocytic tumors (group 1), neuroepithelial tumors other than astrocytic tumors (group 2), and other histopathological tumors (group 3). Group 1 included two diffuse astrocytomas (DAs), six anaplastic astrocytomas (AAs), and 23 glioblastomas. Group 2 included three oligoastrocytomas (OAs), one oligodendroglioma (OL), one central neurocytoma, one anaplastic ependymoma (AE), two anaplastic oligoastrocytomas (AOAs), eight anaplastic oligodendrogliomas (AOs), and five glioblastomas with an oligodendroglial component (glioblastoma with oligo). Group 3 included seven primary central nerve system lymphomas (PCNSLs), two metastatic brain tumors, one craniopharyngioma, one hamartoma, one hemangioblastoma, one atypical meningioma, and one lymphomatoid granulomatosis (LYG) (Table 1).

Table 1	ALL	Group 1	Group 2	Group 3
N	66	25	20	14
Age (range)	27-85	27-85	30-78	32-77
Sex (M:F)	36: 30	12:19	13:7	11:4
Histopathological diagnosis (N)		DA (2) AA (6) glioblastoma(23)	OA (3) OL (1) AE (1) AOA (2) AO (8) glioblastoma with oligo(5) Central neurocytoma (1)	PCNSL (7) LYG (1) Metastatic tumortumor (2) Craniopharyngioma (1) Hamartoma (1) Hemangioblastoma (1) Atypical meningioma (1)

Numbers in parentheses indicate the number of patients.

Assessment of necrosis

Two experienced neuropathologists (Ka.Ha. and Sa.Yu.) assessed each specimen and evaluated the presence of necrosis in consensus. The diagnosis and evaluation were determined by agreement of the two pathologists.

Statistical analysis

All parametric variables are presented as the means ± standard deviation (SD). Mean values of the FMISO TNR were compared between groups by the Welch's t-test. The associations between image analysis and histopathological necrosis were examined by receiver operating characteristic (ROC) analysis. P-values less than 0.05 were considered statistically significant. R 3.1.2 for Windows and the 'survival' package were used for all statistical analyses.

Results

Histopathological necrosis and diagnosis

Histopathological necroses were observed in 23/23 glioblastomas (100%), 5/5 glioblastomas with oligo (100%), 1/8 AOs (12.5%), 1/1 AE (100%), 4/7 PCNSLs (57.1%), and 1/2 metastatic brain tumors (50%), and 1/1 atypical meningioma (100%). Necroses were found in 17/31 cases in group 1, 7/20 cases in group 2, and 6/15 cases in group 3.

TNR and necrosis

The TNR in group 1 was 3.45 ± 0.97 vs. 1.43 ± 0.42 (with vs. without necrosis), the TNR in group 2 was 2.91 ± 0.83 vs. 1.44 ± 0.20, and the TNR in group 3 was 2.63 ± 1.16 vs. 1.36 ± 0.22 (Figure 1). The TNRs of cases with necrosis were significantly higher than those of cases without necrosis in each group (group 1, 2, and 3: $p < 0.00001$, $p < 0.005$, and $p < 0.05$, respectively). The lowest TNR in necrosis positive cases was 1.65.

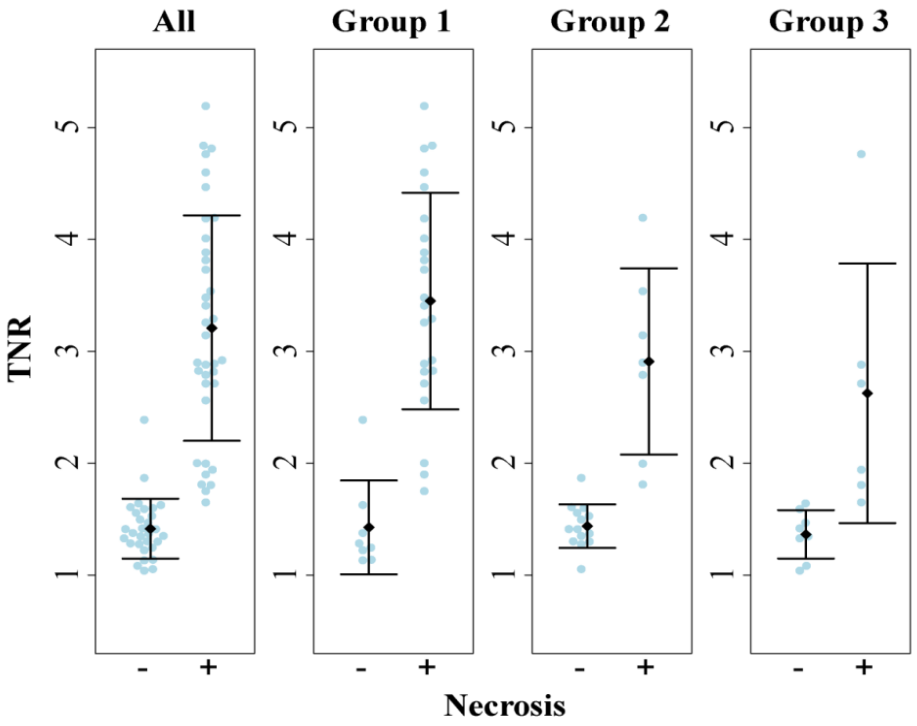

Figure 1. Differences and distribution of FMISO TNRs in group 1, 2, 3, and all groups.

Semi-quantitative analysis

The ROC curve towards necrosis and TNR including all cases is shown in Figure 2. The AUC was 0.989. At the lowest FMISO value of necrosis positive group (TNR = 1.65), the sensitivity, specificity, and accuracy were 100.0%, 93.3%, and 97.0% respectively.

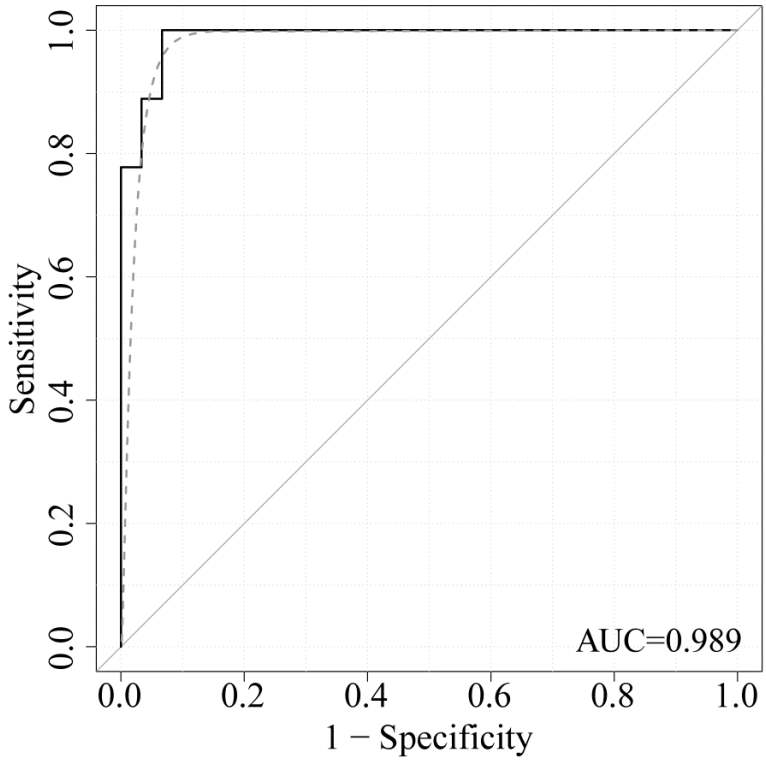

Figure 2. ROC curve for the presence of necrosis generated from TNRs including all cases. The ROC curve showed a very good correlation between necrosis and TNR (AUC=0.989).

Discussion

In this study, semi-quantitative analyses indicated a strong correlation between the FMISO uptake status and the presence of necrosis. The correlations were significant not only in astrocytic tumors, but also in various histological types of brain tumor. It appears that both the presence of intratumoral micro-necrosis and FMISO uptake have certain thresholds of pO2 pressure. Our results of strong agreement between necrosis and FMISO uptake suggest that the thresholds are close to each other. Any specimen form cases with FMISO TNR < 1.65 did not present necrosis. Thus, TNR 1.65 has a potential as a threshold for detecting intratumoral micro-necrosis.

We can also described that FMISO PET could visualize intratumoral microscopic necrosis in vivo. So far, central necrosis is an important finding in malignant brain tumors, and

wide-ranging necrosis can be clearly detected by conventional MRI. However, histological micro-necrosis is also important for the diagnosis of malignant brain tumors, especially glioblastoma, because the presence of micro-necrosis is critical information for glioblastoma diagnosis regardless of imaging central necrosis [14]. In addition, atypical and anaplastic meningiomas frequently have histopathological necrosis, and the patient outcomes of these tumors are usually poorer than those of ordinary meningiomas[13,21].

In this context, FMISO-positive areas might indicate not only severe hypoxic areas (necrotic areas), but also malignant parts of the tumor. FMISO PET might be able to visualize the tumor malignancy in many types of brain tumors. In fact, there are several lines of evidence showing that FMISO-positive lesions are associated with tumor malignancy. These studies indicated that a large volume of hypoxia in glioma measured by FMISO PET is strongly associated with a poorer prognosis[11,12,22,23].

Chapter 2

Purpose

Glioblastoma is the most aggressive astrocytic tumor among cerebral gliomas. It is defined as grade IV according to the 2007 World Health Organization (WHO) classification[14]. Recently, the prognosis of glioblastoma patients has been significantly improved owing to the development of image-guided surgery and radiotherapy and new chemotherapeutic drugs; however, the 2-year survival rate remains at only 27%[24].

Since glioblastomas frequently develop severe hypoxia[10,25-29], many glioblastoma patients underwent FMISO PET which enables the non-invasive detection of hypoxia in vivo[10].

Tumor cells can adapt themselves to hypoxia by promoting the genes which drive glucose metabolism and allow the tumor cells to survive and proliferate in hypoxia. In such conditions, glucose is metabolized without consuming oxygen to produce lactate (anaerobic glycolysis) whereas oxygen is essential to fully metabolize glucose (oxidative phosphorylation)[30]. Hypoxia imaging has been reported to provide prognostic information in glioblastoma patients; for example, previous studies found that glioblastoma patients with a larger HV in the tumor had shorter survival[11,12,22,23]. However, hypoxia imaging may reflect not only active tumor cells but also dying cells that could not survive severe hypoxic conditions[29].

Metabolic activity can be measured using FDG PET. According to previous reports, both the intensity and volume of glucose metabolism was associated with poor prognosis in glioma patients [31-33]. Thus, metabolically active HV can be segmented as the volume showing both FMISO and FDG uptakes. Additionally, because FMISO accumulates in severely hypoxic tissue where normal neurons and glial cells cannot survive, we hypothesized that FDG within FMISO-positive areas all represent tumor metabolism. In the present study, we aimed to investigate the volume of anaerobic glycolysis in relation to patient outcome.

Materials and Methods

Study subjects

Same as the chapter 1, we reviewed 141 patients for the investigation of possible brain tumors. Patients who did not undergo surgery (resection or biopsy) were excluded. Considering the possible modification of metabolism or hypoxia status by interventions, we further excluded patients who had already received any treatments before PET scanning, including anti-cancer chemotherapy, radiotherapy, and tumor resection.

Among them, 32 patients were diagnosed as having glioblastoma. The final study population consisted of 17 male and 15 female glioblastoma patients (age, 63.5±14.8 years). The patients' characteristics' are shown in Table 2. Pathological diagnosis was determined by agreement between two experienced neuropathologists based on the WHO 2007 classification [14]. All of the 32 glioblastoma patients received additional chemoradiotherapy with temozolomide.

Table 2

Characteristic	Value
Age (years)	
Mean SD	63.5±14.8
Median	66.0
Range	27–85
Sex, n	
Male/Female	17/15
KPS	
Median	75
Range	50–100
EOR, %	
Mean SD	63.47±14.81
Median	93.73
Range	0–100
IDH1/2 mutations, n	
–	24
+	1
Unknown	7

Image acquisition and reconstruction

Same as the chapter 1, MRI was conducted to generate the following image series: T1-weighted images with and without gadolinium contrast medium, T2-weighted images, and FLAIR images. FDG and FMISO PET were conducted in random order with an interval of <7 days. Both FDG and FMISO PET protocols were the same as in the chapter 1, with the exception of the types of scanner used. Briefly, for FMISO PET, static PET scanning was initiated at 4 hours after intravenous injection. The actual interval and dosage were 4.06±0.30 hours, and 413.9±28.2 MBq, respectively. On the day of the FDG PET scan, the patients fasted for >6 hours before the study. The static PET images were acquired at 1 hour after intravenous FDG (4.5MBq/kg) injection. The actual interval and dosage were 1.23±0.30 hours, and 323.3±90.6 MBq, respectively.

Image analysis

Definition of volume of interest: FDG and FMISO PET images, and FLAIR and gadolinium-enhanced T1-weighted MR images were co-registered with individual gadolinium-enhanced T1-weighted MR images using SPM8 software. A nuclear medicine physician created the VOIs manually to enclose the entire area showing gadolinium enhancement as the gross tumor volume (GTV), and to enclose the entire area exhibiting a high intensity of FLAIR in the tumor lesion. Every VOI was created using an application tool that was developed in our institute. Polygonal ROIs were drawn on all the slices that showed gadolinium enhancement of the tumor. The boundaries of the ROIs were made 3–5 mm outside of the Gd enhancement area to include all of the gadolinium-enhanced voxels in the ROIs. The VOI was generated by integrating all of the polygonal ROIs as the tumor lesion.

The normal reference regions were identified on the gadolinium-enhanced T1-weighted MR images of each patient. Contralateral frontal and parietal cortices were used as the reference region in the case of FDG, whereas cerebellar cortex was used as the reference region in the case of FMISO. Circular ROIs (10 mm in diameter) were placed in the manner described as follows.1) For FMISO, we placed 30 ROIs on the cerebellar cortex same as the chapter 1. The averaged value was used for the reference. 2) For FDG, we placed six ROIs on each of the three axial slices on the contralateral frontoparietal cortex. The averaged value was used for the reference. Another nuclear medicine physician visually confirmed that all tumoral and normal ROIs were defined appropriately. Both nuclear medicine physicians had completed neuroradiology training in our institute. The TNR was calculated by dividing the maximum SUV of the tumor lesions by the averaged SUV of normal reference. For FMISO, we averaged cerebellar uptake for the normal reference, because use of target-to-cerebellum ratio has been recommended to most accurately approximate distribution volume [34]. For FDG reference, cerebellum is not appropriate because the cerebellum cortex uptake is often reduced by contralateral supratentorial tumor (so called crossed cerebellar diaschisis or CCD). Instead, contralateral cortex, which we used in this study, has been commonly adopted for FDG normal reference.

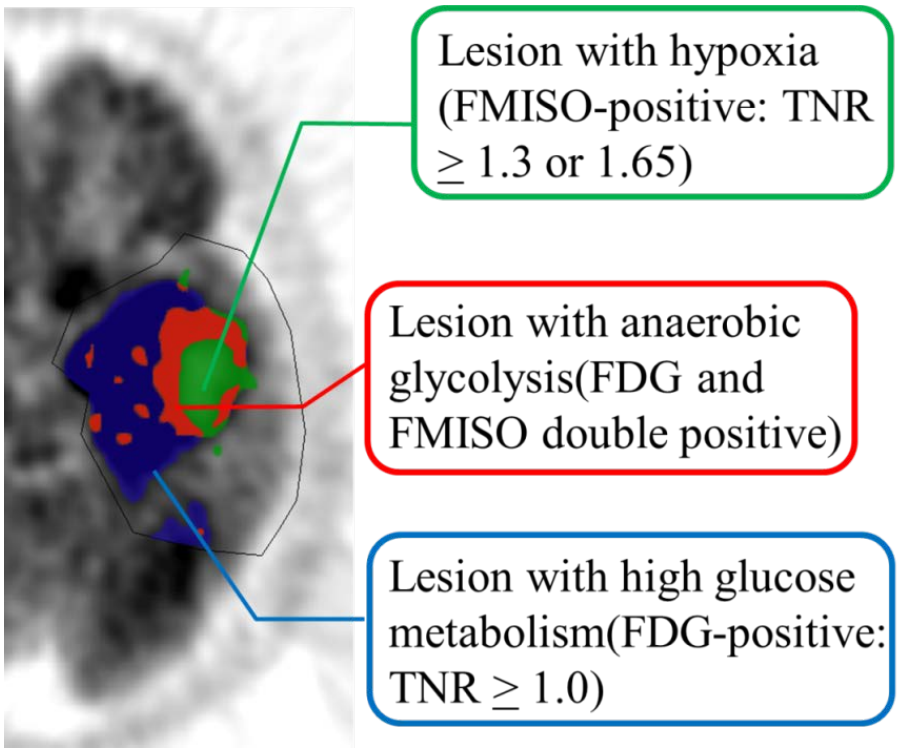

Figure 3. The example of lesion definition for image analysis. Blue represent lesion with high glucose metabolism, green represent lesion with hypoxia, and, red represent lesion with anaerobic glycolysis.

Volume definition: Within the VOIs with FLAIR high intensity, a voxel that had an FMISO TNR ≥1.3 or 1.65 was defined as FMISO-positive; this was because we successfully detected tumor hypoxia in our previous study [10] or the chapter 1. The FMISO-positive region was considered as the HV. The voxel having an FDG TNR ≥1.0 was defined as FDG-positive. Metabolic tumor volume (MTV) measurement for brain tumor is interfered by physiological FDG uptake in the surrounding brain tissues. Thus, here we propose a new parameter, namely hypoxic MTV (hMTV), which is the volume showing as FMISO-positive and FDG-positive (Figure 3). Here, we define hypoxic total lesion glycolysis (hTLG) as [hMTV]×[SUVmean within hMTV]. The hypermetabolic fraction of hypoxia volume (HMF) was defined as [hMTV]/[HV]. The GTV, HV, hMTV, hTLG, and HMF were examined in relation to patient outcome. Subscripted number of HV, hMTV, hTLG, and HMF(i.e., $_{1.3}$ or $_{1.65}$) are represented the applied FMISO threshold (i.e., FMISO TNR $\geq$ 1.3 or 1.65) to detect the FMISO- positive voxel.

Extent of resection

The surgical procedure was same as chapter 1. The extent of resections (EOR) using cytoreduction surgery was quantitatively estimated by volumetric change based on planimetry methods using a conventional 6–7-mm-thick slice of Gd-T1WI MRI as described previously[35]. Pre- and post-operative tumor volumes were calculated as the sum of the Gd-enhanced area that was determined manually; then the resected tumor volume was determined by subtraction of the post-operative tumor volume from the pre-operative tumor volume. The EOR was defined as the percentage of resected tumor volume in the pre-operative tumor volume. Post-operative tumor volumes were assessed using Gd-T1WI MRI that was performed at <48 hours after surgery to avoid post-operative changes showing Gd enhancement. In needle biopsy cases, the EOR were defined as 0%. In total, 19, 6, and 7 patients underwent sub-total or gross-total resection (EOR=90.3-100%), partial resection (EOR=10.6-85.5%), and biopsy (EOR=0-2.1%), respectively.

Prognosis

Overall survival (OS) was defined as the time period (months) between the date of surgery and the date of death for any reason. Progression-free survival (PFS) was defined as the time period (months) between the date of surgery and the date that tumor recurrence was confirmed using any imaging modalities. We observed all patients for >2 months or until death. Twenty-four patients experienced tumor recurrence, 20 of whom died during the follow-up period (OS=3.2-46.8 months). The remaining 8 patients without recurrence were all alive at the end of the follow-up period, resulting in a total of 12 patients being alive at the end of the follow-up period (2.7-45.1 months).

Statistical analysis

All continuous variables are presented as the mean ± standard deviation. In this study, we attempted to exhaustively determine the optimal cutoff values for each parameter to best categorize patients by OS. We repeatedly applied the log-rank test to each parameter and decided the optimal cutoff values that showed maximum $\chi 2$ statistics. This method was applied to the TNR, GTV, HV, hMTV, hTLG, HMF, EOR, Karnofsky performance status and patient age. The survival curves were created using the Kaplan–Meier method. We tested the correlation between PFS or OS and parameters using the Cox regression model for univariate analysis and with the Cox proportional hazard model for multivariate analysis. To avoid a problem of multiple testing, the p values of univariate analyses were corrected by the method which was previously reported [36].

All the statistical analyses were performed using R version 3.1.2 and ‘survival’ add-on

package. P values of <0.05 were considered statistically significant.

Results

SUVmax and tumor volumes

The SUVmax for FDG was 8.44±3.00 (range, 4.19–15.03), the TNR for FDG was 1.55±0.52 (range, 1.08–3.96). All (100%) of the lesions had a higher FDG SUVmax than the reference value (i.e., TNR≥1.0), and thus were considered to have a hypermetabolic volume in the tumor. The SUVmax for FMISO was 3.75±1.30 (range, 1.71–6.91), and the TNR for FMISO was 3.29±0.81 (range, 1.48–4.85). In volumetric assessment, the $hMTV_{1.3}$ and $HV_{1.3}$ were 7.98±8.85ml (range, 0.12–35.27 ml) and 29.78±18.90 (range, 0.84–81.95 ml), respectively. The $hTLG_{1.3}$ was 41.69±37.65 (range, 0.66–126.26), and the $HMF_{1.3}$ was 25.15±18.03% (range, 0.89–61.80%).

The volumetric parameters with FMISO TNR threshold $\geq$ 1.65 was shown in Table 3.

Table 3

	Mean±SD	range
$HV_{1.65}$ (ml)	15.69±31.81	0.00-49.91
$hMTV_{1.65}$ (ml)	6.03±6.87	0.00-26.03
$hTLG_{1.65}$ (ml)	31.64±31.07	0.00-114.56
$HMF_{1.65}$ (%)	36.52±25.25	0.00-80.64

Univariate analysis

Table 2 summarizes the optimal cutoff values that generated maximum χ^2 statistics for each parameter in categorizing patients by OS. At these cutoff values, the $hMTV_{1.3}$, $hTLG_{1.3}$, and EOR were significantly correlated with PFS (p=0.007, p=0.04, and p=0.01, respectively) using univariate analysis. A significantly shorter OS was also suggested by higher $HV_{1.3}$, higher $hMTV_{1.3}$, higher $hTLG_{1.3}$, and lower EOR (p=0.04, p=0.0028, p=0.037, and p=0.014, respectively) (Table 4). None of parameters with FMISO threshold settled at 1.65 (i.e., $HV_{1.65}$, $hMTV_{1.65}$, $hTLG_{1.65}$) successfully separated the patients between short OS vs. long OS or between short PFS vs. long PFS. For OS, the corrected p values for $HV_{1.65}$, $hMTV_{1.65}$, and $hTLG_{1.65}$ were 0.15, 0.081, and 0.17, respectively. Similarly for PFS, the corrected p values were 0.73, 0.088, 0.21, respectively). Seven patients with a higher $hMTV_{1.3}$ (i.e., $hMTV_{1.3} \geq 15.01$) had a significantly shorter OS than the remaining 25 patients with a lower hMTV (i.e., $hMTV_{1.3} < 15.01$); the median OS was 5.3 months for the high $hMTV_{1.3}$ group (n=7) vs. 15.7 months for the low $hMTV_{1.3}$ group

(n=25). Twelve patients with a higher $hTLG_{1.3}$ (i.e., $hTLG_{1.3} \geq 49.41$) had a significantly shorter OS than the remaining 20 patients with a lower $hTLG_{1.3}$ (i.e., $hTLG_{1.3} < 49.41$); the median OS was 5.8 months for the high $hTLG_{1.3}$ group (n=12) vs. 15.7 months for the low $hTLG_{1.3}$ group (n=20) (Figure 4). Sixteen patients with a higher EOR (i.e., EOR≥94.5%) had a significantly longer OS than those with a lower EOR (i.e., EOR <94.5%); the median OS was 21.6 months for the low-EOR group (n= 16) vs. 11.3 months for the low-EOR group (n= 16) in common with previous reports.

Table 4

	PFS		OS	
	p value	HR	p value	HR
FMISO TNR	1.0	1.44 (0.47-4.38)	1.0	1.52 (0.43-5.38)
FDG TNR	0.26	2.23 (0.95-5.26)	0.64	1.81 (0.72-4.54)
GTV (ml)	1.00	1.18 (0.27-5.24)	0.14	3.49 (0.67-18.09)
$HV_{1.3}$ (ml)	0.89	1.71 (0.62-4.69)	**0.040**	**4.65 (1.53-13.19)**
$HMF_{1.3}$ (%)	0.23	2.57 (0.97-6.77)	0.22	2.67 (0.99-7.21)
$hMTV_{1.3}$ (ml)	**0.0070**	**7.11 (2.23-22.66)**	**0.0028**	**19.93 (3.90-101.96)**
hTLG (ml)	**0.040**	**3.86 (1.45-10.27)**	**0.037**	**4.28 (1.51-12.15)**
age (y.o.)	1.00	1.04 (0.43-2.55)	1.0	0.94 (0.31-2.87)
KPS	0.50	1.89 (0.79-4.49)	0.34	2.82 (0.88-5.36)
EOR(%)	**0.010**	**0.23 (0.092-0.56)**	**0.014**	**0.13 (0.036-0.47)**

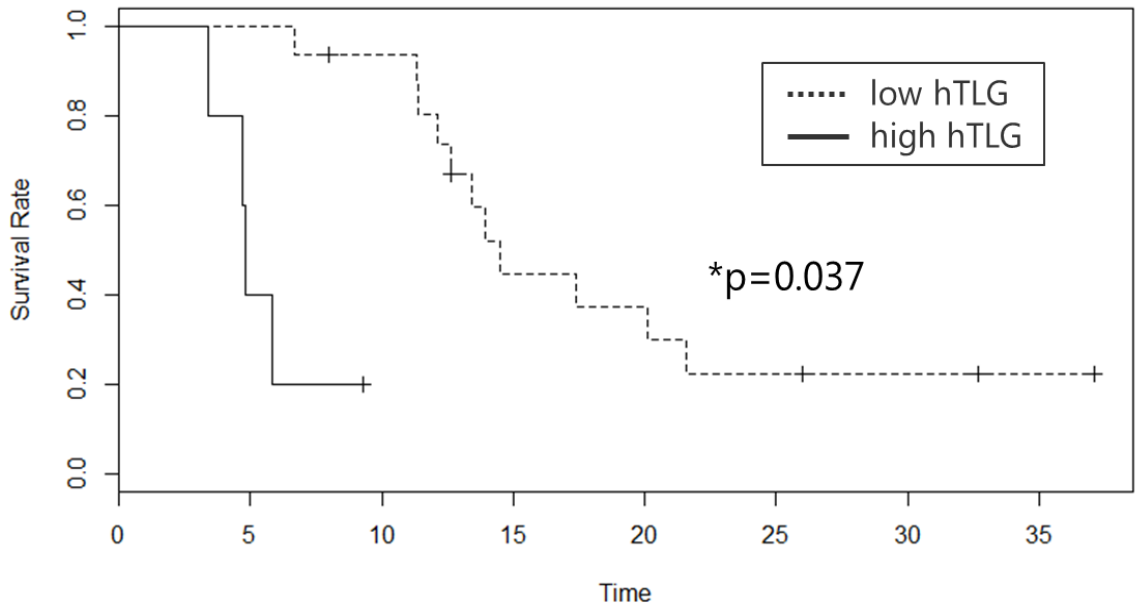

Figure 4. Kaplan-Meier curves for patient's OS. Patients with a higher hTLG had a significantly shorter OS.

Multivariate analysis

Because the $hMTV_{1.3}$ and $hTLG_{1.3}$ were significantly correlated (Pearson's R=0.90; p<0.0001), we constructed two separate models to avoid the co-linearity problem. Model 1 consisted of the $hMTV_{1.3}$ + $HV_{1.3}$ + EOR, and model 2 consisted of the $hTLG_{1.3}$ + $HV_{1.3}$ + EOR. The Cox proportional hazard model for $hMTV_{1.3}$, $HV_{1.3}$, and EOR used to predict OS (model 1) indicated that the $hMTV_{1.3}$ and EOR were independent prognostic factors (p=0.0063 and p=0.013, respectively; Table 5a). Analysis using model 2 similarly suggested that the $hTLG_{1.3}$ and EOR independently affected OS (p=0.011 for $hTLG_{1.3}$ and p=0.0042 for EOR; Table 5b). PFS was also independently influenced by the $hMTV_{1.3}$ or $hTLG_{1.3}$ (Table 5).

Table 5a

	Model 1 :PFS or OS~HV+hMTV+EOR			
	PFS		OS	
	p value	HR	p value	HR
HV (ml)	1.00	1.00 (0.33-3.08)	0.21	2.069 (0.66-6.50)
hMTV (ml)	**0.0020**	**6.68 (2.01-22.24)**	**0.0063**	**10.45 (1.94-56.27)**
hTLG (ml)				
EOR(%)	**0.0074**	**0.26 (0.097-0.70)**	**0.0042**	**0.12 (0.029-0.52)**

Table 5b

	Model 2 : PFS or OS~HV+hTLG+EOR			
	PFS		OS	
	p value	HR	p value	HR
HV (ml)	0.49	0.68 (0.23-2.04)	0.50	1.51 (0.46-4.98)
hMTV (ml)				
hTLG (ml)	**0.027**	**3.07 (1.13-8.33)**	**0.011**	**5.64 (1.49-21.42)**
EOR(%)	**0.0032**	**0.22 (0.082-0.60)**	**0.013**	**0.18 (0.046-0.70)**

Discussion

We conducted a study involving the independent detection of hypermetabolic and hypoxic volumes using FDG PET and FMISO PET, respectively. The parameters $hMTV_{1.3}$ and

$hTLG_{1.3}$ were tested as prognostic factors. Using univariate analysis we found that the patients who had a larger $hMTV_{1.3}$ or larger $hTLG_{1.3}$, or had undergone a more extensive surgical procedure, survived significantly longer than the other patients. In addition, multivariate analysis indicated that both the $hTLG_{1.3}$ and $hMTV_{1.3}$ were significant prognostic factors that were independent from the EOR. However, none of parameters by threshold of FMISO TNR 1.65 reached statistical significance to predict patients' prognosis. While the FMISO TNR 1.65 may be a good threshold for detecting intratumoral microscopic necrosis, different cut-off values should be applied for delineating hypoxic area.

Recent studies have reported that a lower EOR was a predictor of poor prognosis in glioma patients[16,37-41]. Our study confirmed this finding. In addition to the EOR, we newly found that the $hTLG_{1.3}$ and $hMTV_{1.3}$ may predict patient prognosis.

In malignant tumor cells, especially under severely hypoxic conditions, HIF-1α is often promoted through signal transductional pathways, such as the phosphoinositide-3-kinase/Akt/mTOR pathway, extracellular regulated protein kinase pathway, and adenosine 5′ -monophosphate activated protein kinase pathway. HIF-1α forms a complex with HIF-1β or with other proteins, and adheres to HRE on the genome line. HRE stimulates the downstream enzymes in the glycolytic system such as glucose transporters, hexokinase, pyruvate kinase, and lactate dehydrogenase A[42]. This cascade helps tumor cells metabolize glucose anaerobically and survive under severe hypoxia, the so called Warburg effect.

In the chapter 2, we hypothesized that FDG uptake intensity in the hypoxic area (i.e., the FMISO-positive area) could represent the tumor's ability to adapt to severe hypoxia. In other words, the FDG/FMISO double-positive fraction may reflect 'signal transmission efficiency' initiated from hypoxia to anaerobic glycolysis. Therefore, we investigated the intensity of anaerobic glycolysis by using the new parameters $hMTV_{1.3}$ and $hTLG_{1.3}$.

Summary and Conclusion

1. FMISO uptake represents presence of microscopic necrosis.
2. The hMTV and hTLG may be new prognostic parametors in glioblastoma patients as a tumoral anaerobic glycolysis.

In chapter 1, FMISO PET could visualize intratumoral microscopic necrosis in vivo and could provide important information for treatment decisions and surgical strategies of any type of brain tumor. The presence of micro-necrosis is critical information especially for glioma, atypical meningiomas, and anaplastic meningiomas. The patient outcomes of

these tumors with histopathological necrosis are usually poorer than without necrosis. Thus, FMISO-positive areas might indicate not only severe hypoxic areas, but also malignant parts of the tumor. Clinical application of FMISO PET is providing important information for biopsy to determine the biopsy site as well as accurate diagnosis of the histological malignancy of these tumors.

In chapter 2, the combination of FDG and FMISO PET may allow evaluate tumoral anaerobic glycolysis. We introduced hMTV and hTLG as parameters of anaerobic glucose metabolism for glioblastoma patients, and both were significant predictors for OS in glioblastoma patients. These prognostic factors might be independent from the EOR. The point is that we can determine these parameters during the pre-treatment phase. These findings may provide the necessary information for the detection of the patients who will develop early recurrence regardless of the surgical procedure. Such patients might be considered eligible for additional treatment in the future, such as expanding resection of the non-eloquent area, radiation dose escalation, hypoxia-activated chemotherapy, immunotherapy, or photodynamic therapy.

In summary, FMISO PET can visualize microscopic necrosis and anaerobic glycolysis both reflecting tumor malignancy.

Limitations and future direction

We need to mention the limitations regarding the study. First, the number of patients enrolled was small. In chapter 1, the tolerance to hypoxia might be different among histopathological features. Further studies, especially of non-glioma patient populations, are necessary to verify our results. In chapter 2, although survival analysis was limited, the number of variables making up the multivariate models was reasonable; this was confirmed by a co-author who is an experienced statistician.

Second, the PET images investigated were acquired using several types of PET scanners. The differences in spatial resolution and image contrast may have affected the analyses. However, to minimize these effects, the images were reconstructed using appropriate smoothing filters to match the full width at half maximum of the reconstructed images with each other.

Further studies will be needed to investigate a large number of patients from multiple institutes to confirm and validate the current results in the future. To support our results, we also should assess the biological evidence, like as protein expression, gene mutations, and any other differences in histological samples from different lesions depending on the hypoxia and glycolysis intensity.

謝辞（Acknowledgements）

本研究の遂行にあたり、終始ご指導、ご助言を頂きました核医学分野 教授 玉木長良先生、当学位論文にかかわる 2 編の原著論文の責任著者を務めて頂き、採択まで導いて下さった脳神経外科 特任助教(分子・細胞イメージング部門機能画像科学分野　特任助教兼任)山口秀先生、核医学分野 助教 平田健司先生、すべての病理検体を一から共に見直して下さった北海道大学病院病理部 助教 畑中佳奈子先生、旭川医科大学病院病理部 医員 湯澤明夏先生、FMISO の基礎的な動態に関し、薬理学的な背景をご教授賜りました応用分子画像科学分野 教授 久下裕司先生、脳神経外科の多くの臨床経験を惜しみなくご共有下さった脳神経外科 准教授 寺坂俊介先生、脳神経外科 講師 小林浩之先生、病理学的視点からご指導頂きました腫瘍病理学分野 教授 田中伸哉先生、統計解析手法に関して何度もご指導賜りました医学統計分野 准教授 伊藤陽一先生、毎症例の臨床診断と画像所見に関してご指導頂きました機能画像科学分野 特任助教 小林健太郎先生、原著論文の方向性や考察に関しまして多数のご意見を頂きました核医学分野 准教授 志賀哲先生、LSI 札幌クリニック 院長 服部直也先生、核医学分野 非常勤講師 真鍋治先生、核医学分野 医員 渡邊史郎先生、ならびに各研究室員、病院職員に心より感謝いたします。また、症例の蓄積にご協力頂きました関連各医療機関のご尽力に、心より御礼申し上げます。

References

1 Schofield, C. J. & Ratcliffe, P. J. Oxygen sensing by HIF hydroxylases. *Nature reviews. Molecular cell biology* **5**, 343-354 (2004).

2 Meijer, T. W., Kaanders, J. H., Span, P. N. & Bussink, J. Targeting hypoxia, HIF-1, and tumor glucose metabolism to improve radiotherapy efficacy. *Clinical cancer research : an official journal of the American Association for Cancer Research* **18**, 5585-5594 (2012).

3 Groussard, C. *et al.* Free radical scavenging and antioxidant effects of lactate ion: an in vitro study. *Journal of applied physiology* **89**, 169-175 (2000).

4 Sundar, S. J., Hsieh, J. K., Manjila, S., Lathia, J. D. & Sloan, A. The role of cancer stem cells in glioblastoma. *Neurosurgical focus* **37**, E6 (2014).

5 Urtasun, R. *et al.* Radiation and high-dose metronidazole in supratentorial glioblastomas. *The New England journal of medicine* **294**, 1364-1367 (1976).

6 Dische, S. Chemical sensitizers for hypoxic cells: a decade of experience in clinical radiotherapy. *Radiotherapy and oncology : journal of the European Society for Therapeutic Radiology and Oncology* **3**, 97-115 (1985).

7 Van Os-Corby, D. J., Koch, C. J. & Chapman, J. D. Is misonidazole binding to mouse tissues a measure of cellular pO2? *Biochemical pharmacology* **36**, 3487-3494 (1987).

8 Rasey, J. S., Nelson, N. J., Chin, L., Evans, M. L. & Grunbaum, Z. Characteristics of the binding of labeled fluoromisonidazole in cells in vitro. *Radiation research* **122**, 301-308 (1990).

9 Kavanagh, M. C., Sun, A., Hu, Q. & Hill, R. P. Comparing techniques of measuring tumor hypoxia in different murine tumors: Eppendorf pO2 Histograph, [3H]misonidazole binding and paired survival assay. *Radiation research* **145**, 491-500 (1996).

10 Hirata, K. *et al.* (1)(8)F-Fluoromisonidazole positron emission tomography may differentiate glioblastoma multiforme from less malignant gliomas. *European journal of nuclear medicine and molecular imaging* **39**, 760-770 (2012).

11 Spence, A. M. *et al.* Regional hypoxia in glioblastoma multiforme quantified with [18F]fluoromisonidazole positron emission tomography before radiotherapy: correlation with time to progression and survival. *Clinical cancer research : an official journal of the American Association for Cancer Research* **14**, 2623-2630 (2008).

12 Kawai, N. *et al.* Correlation between (1)(8)F-fluoromisonidazole PET and

expression of HIF-1alpha and VEGF in newly diagnosed and recurrent malignant gliomas. *European journal of nuclear medicine and molecular imaging* **41**, 1870-1878 (2014).

13 Moradi, A. *et al.* Pathodiagnostic parameters for meningioma grading. *Journal of clinical neuroscience : official journal of the Neurosurgical Society of Australasia* **15**, 1370-1375 (2008).

14 Louis, D. N. *et al.* The 2007 WHO classification of tumours of the central nervous system. *Acta neuropathologica* **114**, 97-109 (2007).

15 Miller, C. R., Dunham, C. P., Scheithauer, B. W. & Perry, A. Significance of necrosis in grading of oligodendroglial neoplasms: a clinicopathologic and genetic study of newly diagnosed high-grade gliomas. *Journal of clinical oncology : official journal of the American Society of Clinical Oncology* **24**, 5419-5426 (2006).

16 Lacroix, M. *et al.* A multivariate analysis of 416 patients with glioblastoma multiforme: prognosis, extent of resection, and survival. *Journal of neurosurgery* **95**, 190-198 (2001).

17 Grunbaum, Z. *et al.* Synthesis and characterization of congeners of misonidazole for imaging hypoxia. *Journal of nuclear medicine : official publication, Society of Nuclear Medicine* **28**, 68-75 (1987).

18 Thorwarth, D., Eschmann, S. M., Paulsen, F. & Alber, M. A kinetic model for dynamic [18F]-Fmiso PET data to analyse tumour hypoxia. *Physics in medicine and biology* **50**, 2209-2224 (2005).

19 Yamaguchi, S. *et al.* Detection of histological anaplasia in gliomas with oligodendroglial components using positron emission tomography with (18)F-FDG and (11)C-methionine: report of two cases. *Journal of neuro-oncology* **101**, 335-341 (2011).

20 Kobayashi, K. *et al.* Prognostic value of volume-based measurements on (11)C-methionine PET in glioma patients. *European journal of nuclear medicine and molecular imaging* **42**, 1071-1080 (2015).

21 Yamaguchi, S. *et al.* Prognostic factors for survival in patients with high-grade meningioma and recurrence-risk stratification for application of radiotherapy. *PloS one* **9**, e97108 (2014).

22 Szeto, M. D. *et al.* Quantitative metrics of net proliferation and invasion link biological aggressiveness assessed by MRI with hypoxia assessed by FMISO-PET in newly diagnosed glioblastomas. *Cancer research* **69**, 4502-4509 (2009).

23 Swanson, K. R. *et al.* Complementary but distinct roles for MRI and 18F-

fluoromisonidazole PET in the assessment of human glioblastomas. *Journal of nuclear medicine : official publication, Society of Nuclear Medicine* **50**, 36-44 (2009).

24 Omuro, A. & DeAngelis, L. M. Glioblastoma and other malignant gliomas: a clinical review. *Jama* **310**, 1842-1850 (2013).

25 Flynn, J. R. *et al.* Hypoxia-regulated protein expression, patient characteristics, and preoperative imaging as predictors of survival in adults with glioblastoma multiforme. *Cancer* **113**, 1032-1042 (2008).

26 Oliver, L., Olivier, C., Marhuenda, F. B., Campone, M. & Vallette, F. M. Hypoxia and the malignant glioma microenvironment: regulation and implications for therapy. *Current molecular pharmacology* **2**, 263-284 (2009).

27 Evans, S. M. *et al.* Hypoxia is important in the biology and aggression of human glial brain tumors. *Clinical cancer research : an official journal of the American Association for Cancer Research* **10**, 8177-8184 (2004).

28 Lally, B. E. *et al.* The interactions of polarographic measurements of oxygen tension and histological grade in human glioma. *Cancer journal* **12**, 461-466 (2006).

29 Toyonaga, T. *et al.* F-fluoromisonidazole positron emission tomography can predict pathological necrosis of brain tumors. *European journal of nuclear medicine and molecular imaging* (2016).

30 Jensen, R. L. Brain tumor hypoxia: tumorigenesis, angiogenesis, imaging, pseudoprogression, and as a therapeutic target. *Journal of neuro-oncology* **92**, 317-335 (2009).

31 Colavolpe, C. *et al.* Independent prognostic value of pre-treatment 18-FDG-PET in high-grade gliomas. *Journal of neuro-oncology* **107**, 527-535 (2012).

32 Spence, A. M. *et al.* 2-[(18)F]Fluoro-2-deoxyglucose and glucose uptake in malignant gliomas before and after radiotherapy: correlation with outcome. *Clinical cancer research : an official journal of the American Association for Cancer Research* **8**, 971-979 (2002).

33 Pardo, F. S. *et al.* Correlation of FDG-PET interpretation with survival in a cohort of glioma patients. *Anticancer research* **24**, 2359-2365 (2004).

34 Bruehlmeier, M., Roelcke, U., Schubiger, P. A. & Ametamey, S. M. Assessment of hypoxia and perfusion in human brain tumors using PET with 18F-fluoromisonidazole and 15O-H2O. *Journal of nuclear medicine : official publication, Society of Nuclear Medicine* **45**, 1851-1859 (2004).

35 Yamaguchi, S. *et al.* The impact of extent of resection and histological subtype on

the outcome of adult patients with high-grade gliomas. *Japanese journal of clinical oncology* **42**, 270-277 (2012).

36 Altman, D. G., Lausen, B., Sauerbrei, W. & Schumacher, M. Dangers of using "optimal" cutpoints in the evaluation of prognostic factors. *Journal of the National Cancer Institute* **86**, 829-835 (1994).

37 Sanai, N. & Berger, M. S. Glioma extent of resection and its impact on patient outcome. *Neurosurgery* **62**, 753-764; discussion 264-756 (2008).

38 Sanai, N., Polley, M. Y., McDermott, M. W., Parsa, A. T. & Berger, M. S. An extent of resection threshold for newly diagnosed glioblastomas. *Journal of neurosurgery* **115**, 3-8 (2011).

39 Keles, G. E., Anderson, B. & Berger, M. S. The effect of extent of resection on time to tumor progression and survival in patients with glioblastoma multiforme of the cerebral hemisphere. *Surgical neurology* **52**, 371-379 (1999).

40 Hardesty, D. A. & Sanai, N. The value of glioma extent of resection in the modern neurosurgical era. *Frontiers in neurology* **3**, 140 (2012).

41 Marko, N. F. *et al.* Extent of resection of glioblastoma revisited: personalized survival modeling facilitates more accurate survival prediction and supports a maximum-safe-resection approach to surgery. *Journal of clinical oncology : official journal of the American Society of Clinical Oncology* **32**, 774-782 (2014).

42 Gao, J. L. & Chen, Y. G. Natural Compounds Regulate Glycolysis in Hypoxic Tumor Microenvironment. *BioMed research international* **2015**, 354143 (2015).